RSC Applied Polymers

Accepted Manuscript

This article can be cited before page numbers have been issued, to do this please use: X. Xiong, S. Anthony, J. Eberhardt, S. Rosenfeldt, D. Friedrich, S. peiffer, J. C. Brendel, J. Breu and T. Lueders, *RSC Appl. Polym.*, 2026, DOI: 10.1039/D6LP00059B.

ROYAL SOCIETY OF CHEMISTRY

rsc.li/RSCApplPolym

View Article Online
DOI: 10.1039/D6LP00059B

Sustainable Barrier Coatings for Food Packaging with a Built-in, Redox-activated Trigger for Surface Hydrophilization

Xiong Xiong,[a] Sulari Anthony,[b] Juliane Eberhardt,[c] Sabine Rosenfeldt,[d] Daniel Friedrich, [a] Stefan Peiffer,[e] Johannes C. Brendel,[c] Tillmann Lueders,*[b] Josef Breu*[a]*

a. University of Bayreuth, Bavarian Polymer Institute and Department of Chemistry, Universitätsstr. 30, 95440 Bayreuth, Germany. E-mail: Josef.breu@uni-bayreuth.de

b. University of Bayreuth, Ecological Microbiology, Bayreuth Center of Ecology and Environmental Research (BayCEER), 95440 Bayreuth, Germany. E-mail: tillmann.lueders@uni-bayreuth.de

c. University of Bayreuth, Macromolecular Chemistry I, 95440 Bayreuth, Germany. E-mail: johannes.brendel@uni-bayreuth.de

d. University of Bayreuth, Physical Chemistry I, Universitätsstr. 30, 95440 Bayreuth, Germany

e. University of Bayreuth, Bayreuth Center of Ecology and Environmental Research (BayCEER), Department of Hydrology, Bayreuth 95440, Germany

ABSTRACT

Plastic pollution, particularly from single use food packaging, has become a significant environmental challenge that requires mitigation by improving degradability in environmental compartments. In this line, a redox-programmable barrier coating is introduced that combines a

View Article Online
DOI: 10.1039/D6LP00059B

high-barrier during usage with a post-use redox-triggered hydrophilization mechanism (Scheme 1).

Fully delaminated vermiculite (VMT) nanosheets were intercalated with poly(*N*-acryloyl thiomorpholine) ($PNAT_{30}$) to form one-dimensional Bragg-stack nanocomposite barrier coatings on poly(lactic acid) (PLA) substrates, yielding highly ordered, 2 μm thin coatings that drastically suppressed oxygen and water vapor transmission to meet state-of-the-art levels for demanding food packaging at elevated relative humidity. Structural Fe(III)/Fe(II) in VMT was furthermore exploited as an intrinsic redox catalyst as followed by Mößbauer spectroscopy under anoxic/oxic cycling. Exposure to active biomass of the Fe(III)-reducing *Geobacter metallireducens* reduced structural Fe(III). Reactive oxygen species (ROS), inferred to form via Fenton-type reactions upon successive reoxygenation, are proposed to oxidize hydrophobic thioether side chains in $PNAT_{30}$ to more hydrophilic sulfoxides, as supported by FTIR, Raman spectroscopy, and solid-state NMR. This molecular transformation triggered a pronounced, stepwise decrease in water contact angle and surface restructuring, evidencing *in situ* formation of a more hydrophilic coating surface. This is expected to increase post-use environmental accessibility and may facilitate eco-corona development and microbial attachment on derived microplastics (MPs), although direct degradation experiments were not performed in the present study. The concept of coupling mineral-induced tortuous-path barrier enhancement with ROS-activated sulfur chemistry provides a generally novel strategy for designing packaging materials that combine excellent in-use protection with a built-in trigger for post-use hydrophilization in redox-fluctuating environmental compartments, such as sewage plants, soils or composting stacks.

KEYWORDS: Microplastic mitigation, Fenton reaction, Bult-in corona formation, Gas barrier.

INTRODUCTION

View Article Online
DOI: 10.1039/D6LP00059B

Plastic pollution has become a systemic problem, with packaging dominating plastic use and waste generation (≈42 % of primary non-fiber plastics are used in packaging, which also represents the largest waste stream).[1] Globally, only about 9 % of plastic waste generated up to 2015 has been recycled, whereas most of the remainder has been landfilled, incinerated, or accumulated in the environment by unintentional or thoughtless littering.[1] Mismanaged waste contributes millions of tons of plastics to soils and the oceans each year, highlighting substantial end-of-life losses for disposable items such as food packaging.[2] Fragmentation and weathering further convert discarded packaging into microplastics (MP)[3] that are now widespread in soils, waters, and living organisms.[4-7] MP clearly has become a vital challenge from scientific, economic, and regulatory perspectives.[8-10] In particular single use food-packaging, which is most prone to littering, must be rendered degradable at the end-of-life.[11-13]

Food packing must protect food mechanically during handling and it must mitigate deterioration of taste or haptics (e.g. crunchiness of chips). Food quality by large determines the best before dates that in turn will lessen food losses.[11] Biodegradable polyesters however have poor barrier properties for both hydrophobic (e.g. O_2, N_2, CO_2) and hydrophilic (H_2O) permeants. Typically, at 25 ℃ and 65 % RH, a 25-µm film of polylactic acid (PLA) shows oxygen (OTR) and water vapor (WVTR) transmission rates of 711 $cm^3\ m^{-2}\ day^{-1}\ atm^{-1}$ and approximately 110 $g \cdot m^{-2} \cdot day^{-1}$, respectively.[14, 15] While extent and rate of swelling with water vapour depend strongly on ester

View Article Online
DOI: 10.1039/D6LP00059B

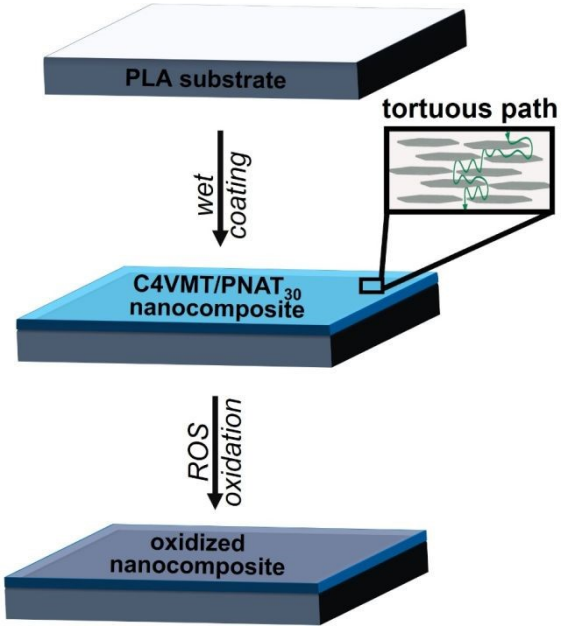

Scheme 1. The C4VMT/PNAT$_{30}$ coating on PLA: assures high-barrier during usage based on establishing a tortuous diffusion path, while in redox-cycling environmental compartments an oxidative surface hydrophilization by reactive oxygen species produced by structural iron is triggered.

type, biodegradable polyesters generally can swell with water to some extent. Water acts like a plasticizer and will increase segment mobility and thus transmission rates not only for H_2O but concomitantly for O_2. Consequently, during usage it is advantageous to have a more hydrophobic polyester. Degradation of biodegradable polyesters is, however, substantially hampered by this hydrophobic nature of the surfaces (Figure S1), that induce slow eco-corona formation to allow enzymatic attack and catabolic mineralization to carbon dioxide and water to become efficient.[16, 17] Formation of an eco-corona can be fostered by a preceding alteration of surfaces by slow photo/thermo-oxidation creating polar groups.[18] Rather than relying on uncontrolled sluggish weathering, a more effective strategy is to introduce oxidation sensitive functionalities into the polymer that can be triggered by conditions changing when the packaging is released into the environment after usage.

Even hydrophobic biodegradable polymers fail to meet barrier specifications for high end food packaging like for potato chips or coffee beans. Only when compounded with high aspect ratio nanosheets, barrier specifications can be met by imposing tortuous diffusion pathways.[19, 20] Here we apply a natural layered silicate, fully delaminated vermiculite (VMT), as a novel barrier filler. Upon utter delamination of VMT into monolayers,[11] nanosheets may be obtained with aspect ratios

View Article Online
DOI: 10.1039/D6LP00059B

of around 9000. As in turn the barrier improvement according to Cussler scales with the square of the aspect ratio, the potential for barrier improvement of VMT[11] is more than 2000 times that of a natural montmorillonite with typical aspect ratio < 200.[20-22] Aside from the thrilling barrier improvement potential, VMT additionally holds promises for post-use surface activation of polymers in environmental compartments: When Fe-bearing 2:1 layered silicates like VMT are exposed to anoxic environments, for instance during composting of food wastes or in sewage plants, structural Fe^{III} will be used as an electron acceptor by anaerobic bacteria.[23] After being re-exposed to oxygen in a subsequent oxic cycle, ROS such as superoxide radicals ($\bullet O_2$) and hydroxyl radicals (•OH) will be produced.[24, 25] As ROS can even cause oxidative cleavage of carbon-carbon bonds in polymers,[26] VMT may not only improve the barrier properties of (bio-)degradable polymers to the level where it meets the benchmarks for sustainable food packaging, but also contribute to post-use surface alteration (chemical aging) of MPs rendering them more hydrophilic and thus potentially more accessible for microbial degradation.[27] In this line, we apply VMT as a catalyst intrinsic to the surface coating that promotes chemical oxidation by ROS generated upon environmental anoxic/oxic cycles.[28] When structural iron in layered silicates is exposed to such redox cycles, Fe(II) produced in the anoxic state upon exposure to O_2 in the oxic state will trigger Fenton-type oxidations even at ambient temperatures.[29] Such redox activity has been utilized in soil remediation and heterogeneous catalysis.[30]

In recent years, redox-responsive polymers have emerged as promising candidates for directing the end of life fate of functional materials.[28, 31-33] Among other reactive groups, these materials exploit reactive sulfur motifs that undergo oxidation converting hydrophobic thioethers (–S–) into hydrophilic sulfoxides (–S(O)–) or sulfones ($–SO_2–$),[28] rendering the polymers more hydrophilic and more prone to swelling with water. In this line poly(*N*-acryloyl thiomorpholine) (PNAT) was

View Article Online
DOI: 10.1039/D6LP00059B

shown to undergo a hydrophobic-to-hydrophilic conversion upon oxidation by H_2O_2 allowing for dissolution of the initially hydrophobic polymer in water.[34]

Thus, in this work, we combine the two lines of thought detailed above, oxidative hydrophilization of a sulfur containing polymer triggered by ROS production by a compounded natural barrier filler after anaerobic microbial exposure. The contact angle of water with a barrier composite coating of $PNAT_{30}$ filled with VMT on PLA could be substantially lowered by both chemical and microbial reduction of structural iron that upon subsequent exposure to oxygen produced ROS capable of oxidizing (–S–) to (–S(O)–). The delaminated VMT nanosheets not only imposed long tortuous pathways that substantially suppressed O_2 and H_2O transport, but concomitantly structural Fe(III)/Fe(II) redox chemistry activated a built-in formation mechanism of a hydrophilic chemical corona by ROS catalysis.

RESULT AND DISCUSSION

Bragg-stack composite via polymer intercalation and its barrier performance

View Article Online
DOI: 10.1039/D6LP00059B

When butylammonium-VMT (C4VMT) is immersed in N-Methylformamide (NMF) it spontaneously and thermodynamically driven delaminates into monolayer nanosheets. Due to the large diameter of the nanosheets their rotation is hampered even at concentrations as low as 2-wt% and a lamellar liquid crystalline (nematic) suspension is obtained instead of an isotropic suspension.

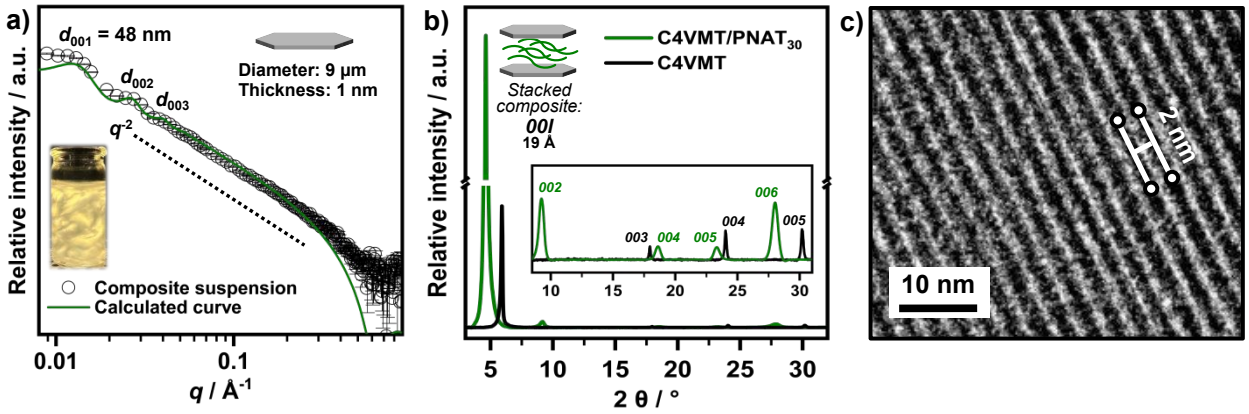

Figure 1. a) SAXS pattern of a 5 wt% C4VMT/PNAT$_{30}$ suspension in NMF. Dotted line shows a q^{-2} scaling. Inset: Photograph of the birefringent suspension under cross-polarized light. b) XRD pattern of a C4VMT film and a dry C4VMT/PNAT$_{30}$ nanocomposite coating. c) TEM image of a cross section of a dry C4VMT/PNAT$_{30}$ nanocomposite coating.

Next the nematic C4VMT suspension is mixed with a solution (2 wt% in dimethylformamide (DMF)) of PNAT$_{30}$ with a low degree of polymerization (30 repeating units) for effective intercalation and minimizing the confinement penalty. The nematic nature of the suspension is preserved upon addition of the polymer solution as indicated by birefringence (Figure 1a inset). Successful delamination and the nematic nature of the suspension was, moreover, cross-checked by the small-angle X-ray scattering (SAXS, Figure 1a). For intensity reasons for this the suspension was concentrated by centrifugation to 5 wt%. The scattering of nanosheets is confirmed by a q^{-2} dependency of the intensity, a *00l* series confirms a co-planar arrangement of nanosheets separated to 48 nm at this concentration, and the lack of a peak at high q values corresponding to C4VMT stacks proves utter delamination. The SAXS pattern was calculated using the model of 1D stacked discs (Figure 1a green line) with a diameter of 9000 nm and a thickness of 1 nm.

View Article Online
DOI: 10.1039/D6LP00059B

The diameter was taken in line with the average diameter of nanosheets as determined by static light scattering (SLS, Figure S2). The liquid crystalline nature of the coating suspension is prerequisite for the perfect texture and the 1D crystalline order of the nanocomposite coating. The liquid crystalline nature is defined by the concentration of the clay in the suspension and the aspect ratio. As the viscosity of the suspension quickly increases with vermiculite concentration, an appreciable aspect ratio is required to assure the nematic nature of the suspension and to obtain the Bragg stack structure and the superb barrier performance related to it.[19, 20]

Nanocomposite coatings with approximately 2 µm dry thickness were applied by doctor-blading a 100-µm thick wet-coat at RT on a PLA film (25 µm).[35, 36] Upon drying at 50°C overnight, the X-ray diffraction (XRD) pattern of the dry coating reveals a 19 Å *d*-spacing (Figure 1b). The observation of a rational *00l* series indicates a one-dimensional (1D) crystalline monodomain of a hybrid Bragg-stack. Upon drying individual VMT nanosheets (1 nm thin) are oriented coplanar to the substrate in a largely overlapping mode with the same amount of polymer volume (0.9 nm thin layers) intercalated between. This ordered polymer intercalation required a careful iterative adjustment of nanosheet to polymer volume with the latter amounting to 47 vol%. The polymer is of course severely confined between the nanosheets. Cross-sectional transition electron micrographs (TEM, Figure 1c) confirm a highly periodic hybrid Bragg-stack structure with uniform interlayer spacing (~2 nm), in excellent agreement with the XRD pattern obtained for the film. According to Cussler models, such textured nanocomposites of large aspect ratio nanosheets substantially elongate the gas diffusion pathway (`tortuous path´) since permeating gas molecules must circumvent thousands of high-aspect-ratio impermeable nanosheets.[19, 20]

The barrier performance of the uncoated PLA film (BoPLA P01001, supplied by Pütz Folien) for O_2 and water vapour is quite moderate,[15] especially at elevated relative humidity.[37, 38] According

View Article Online
DOI: 10.1039/D6LP00059B

to the company´s data sheet a 25 µm PLA foil shows an OTR of 900 $cm^3 \cdot m^{-2} \cdot day^{-1} \cdot bar^{-1}$ (23 °C, 0% RH, ASTM D3985) and a WVTR of 330 $g \cdot m^{-2} \cdot d^{-1}$ (38 °C, 90% RH, ASTM F1249). Values that render neat PLA inappropriate for food packaging.[39] In the present study, PLA was used as a representative biodegradable polyester substrate to evaluate the barrier-enhancing effect of the C4VMT/$PNAT_{30}$ coating. Only the surface modification of the barrier coating was, however, investigated in this study rather than the degradation of the complete packaging including substrate. The 2 µm thin C4VMT/$PNAT_{30}$ Bragg-stack nanocomposite coating substantially improved the barrier. Specifically, the coated PLA film showed an OTR of 1.70 $cm^3 \cdot m^{-2} \cdot day^{-1} \cdot bar^{-1}$ and a WVTR of 1.68 $g \cdot m^{-2} \cdot day^{-1}$ (both measured at 25 °C, 65 % RH). These transmission rates are comparable to values observed for biodegradable nanocomposite coatings made from VMT/PLA nanocomposites and meet even cutting edge food packaging requirements.[11]

View Article Online
DOI: 10.1039/D6LP00059B

$PNAT_{30}$ oxidation by chemically reduced VMT nanosheets

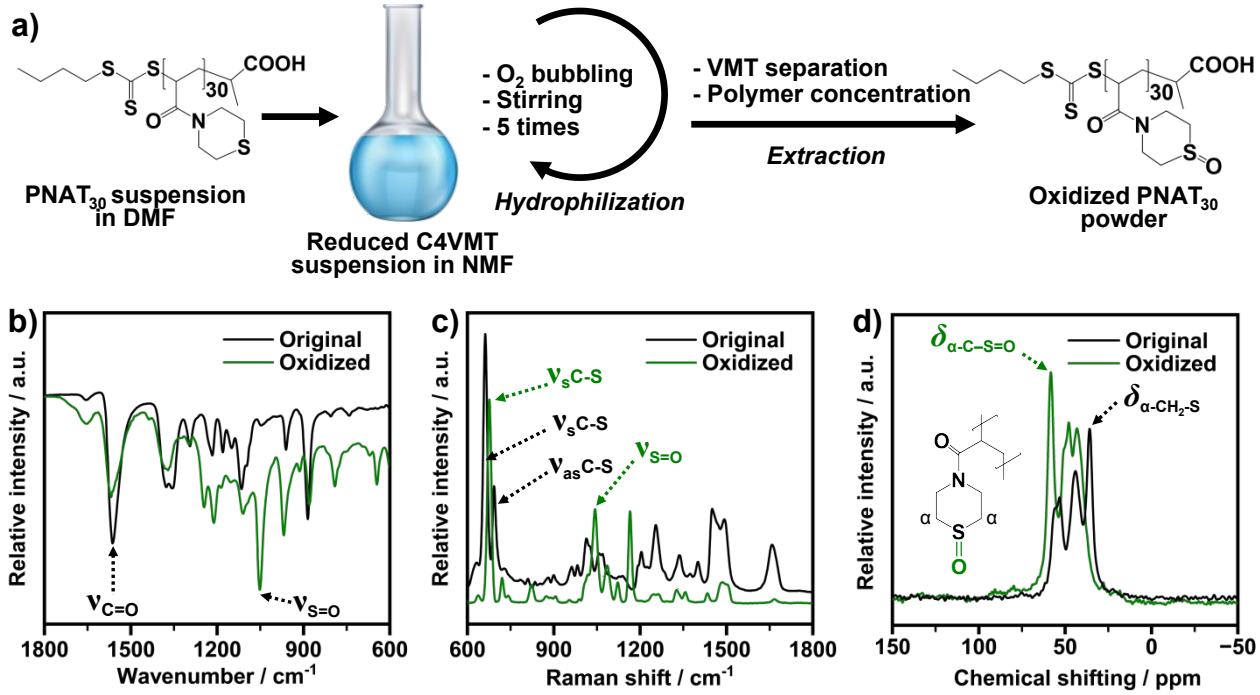

Figure 2. a) Proposed scheme of $PNAT_{30}$ oxidation by ROS inferred to arise during VMT redox cycling. b) FTIR spectra of $PNAT_{30}$ before and after oxidation. c) Raman spectra of $PNAT_{30}$ before and after oxidation. d) ^{13}C CP MAS NMR spectra of $PNAT_{30}$ before and after oxidation. Inset: chemical structure of the oxidized $PNAT_{30}$ repeating unit, highlighting the α-carbon environments corresponding to the assigned resonances.

The biodegradation of MP requires the formation of an eco-corona. For instance, PLA biodegradation primarily occurs through hydrolytic and enzymatic processes by fungi and bacteria, secreting enzymes like polyesterases, esterases, and cutinases that break ester bonds. Fungi such as *Pleurotus, Penicillium*, and *Aspergillus* spp. degrade PLA effectively, with mycelial penetration enhancing substrate access. Coronas (chemically modified surfaces) indirectly affect this by altering PLA surface polarity, potentially facilitating microbial attachment in the plastisphere.[40] As outlined in the introduction, formation of an eco-corona can be fostered by a preceding alteration of surfaces by slow photo/thermo-oxidation creating polar groups.[18] Rather than relying on sluggish uncontrolled weathering, we introduce oxidation sensitive functionalities into the polymer

View Article Online
DOI: 10.1039/D6LP00059B

while applying a VMT barrier filler as an intrinsic catalyst promoting chemical oxidation by ROS generated upon environmental anoxic/oxic cycles.[28]

As the amount of sample in a 2 µm thin coating is minute, we first strived for a prove of concept by blending a solution of $PNAT_{30}$ in DMF with a suspension of reduced C4VMT (R-C4VMT) in NMF. Next, oxidation was abiotically triggered by bubbling O_2 through the suspension (Figure 2a). Upon contact with O_2, structural Fe(II) sites are expected to promote ROS-mediated heterogeneous Fenton-like[41-45] oxidation of thioether units in the $PNAT_{30}$ polymer. The C4VMT was then centrifugated and reduced again exposing the $PNAT_{30}$ polymer to 4 more redox cycles.

The oxidized $PNAT_{30}$ was precipitated by adding acetone as an antisolvent to the DMF/NMF supernatant and finally dried in a vacuum oven at 40°C overnight. Successful oxidation was checked by Fourier transform infrared spectroscopy (FTIR, Figure 2b), where a prominent band at 1051 cm^{-1} indicates a sulfoxide function[46, 47] produced by oxidation of the thioether group. The carbonyl band[51] at ~1633 cm^{-1} and the higher-frequency fingerprint region remained essentially unchanged indicating that the backbone of the polymer remained unaffected. Raman spectroscopy (Figure 2c) provides additional evidence for the oxidative thioether conversion. Upon redox cycling of $PNAT_{30}$, the C–S stretching bands at 630–750 cm^{-1} decreased in intensity, which reflects the gradual conversion of thioether groups. New and strong features appeared in the 1030–1170 cm^{-1} region, which is assigned to the Raman-active S=O vibrations of sulfoxides.[48, 49] Solid-state ^{13}C CP/MAS NMR (Figure 2d) also supported successful oxidation of the thioether group. The main resonance of the α-carbons next to thioether located at 45–50 ppm showed a small but significant downfield shift and an increase in intensity in the oxidized sample. Such spectral changes are in line with previous reports on selective thioether oxidation in polymers and small-molecule analogues.[50] This downfield shift indicates a more electron-withdrawing environment at

View Article Online
DOI: 10.1039/D6LP00059B

α-carbons after oxidation, while the rest of the spectrum remains nearly unchanged. In summary all these spectral features are consistent with selective oxidation of the thioether without changes to the polymer backbone of $PNAT_{30}$ mediated by anoxic/oxic cycling of C4VMT. The oxidation potential of ROS certainly is strong enough to expect further oxidation to sulfone. Experimentally only oxidation to sulfoxide was observed, a fact that is attributed to substoichiometric production of ROS within the limited numbers of redox cycles applied. In the same line, most likely the RAFT end group will also be oxidized, which, however, could not be identified experimentally.

Modification of Surface Hydrophilicity via Redox Cycling of C4VMT/$PNAT_{30}$ Coatings

Next, changes in the wetting angle of C4VMT/$PNAT_{30}$ of barrier coatings were monitored with exposure to environmental anoxic/oxic redox cycling. In line with biotic environmental exposure, cycling was driven by anaerobic bacteria capable of reducing structural iron. After the Bragg-stack coating was prepared, it was completely immersed in a culture medium under strictly anaerobic conditions and inoculated with *Geobacter metallireducens* to trigger biological reduction of structural Fe(III).[51] After at least 24 h, the film was removed from the cultural medium and exposed to the atmosphere for 2 h to activate the Fenton-type oxidation (Figure 3a). ^{57}Fe Mößbauer spectra (Figure 3b, Table S1) recorded before and after exposure to air provided quantitative evidence of partial structural Fe(III) reduction by bacteria under anoxic conditions (Figure 3b, R-C4VMT). While with pristine VMT all structural was Fe(III) (Figure 3b, Pristine VMT), biotic reduction produces an octahedral Fe(II) doublet (red line, chemical shift (CS): 1.51 mm/s, quadrupole splitting (QS): 2.88 mm/s), which is within the expected range for structural Fe(II) in layered

View Article Online
DOI: 10.1039/D6LP00059B

silicates.[52-54] Time-resolved monitoring of the Fe(II) fraction (Figure 3c, Table S2) showed a rapid increase approaching saturation after 24 h, where 24 % of structural Fe(III) has been reduced.

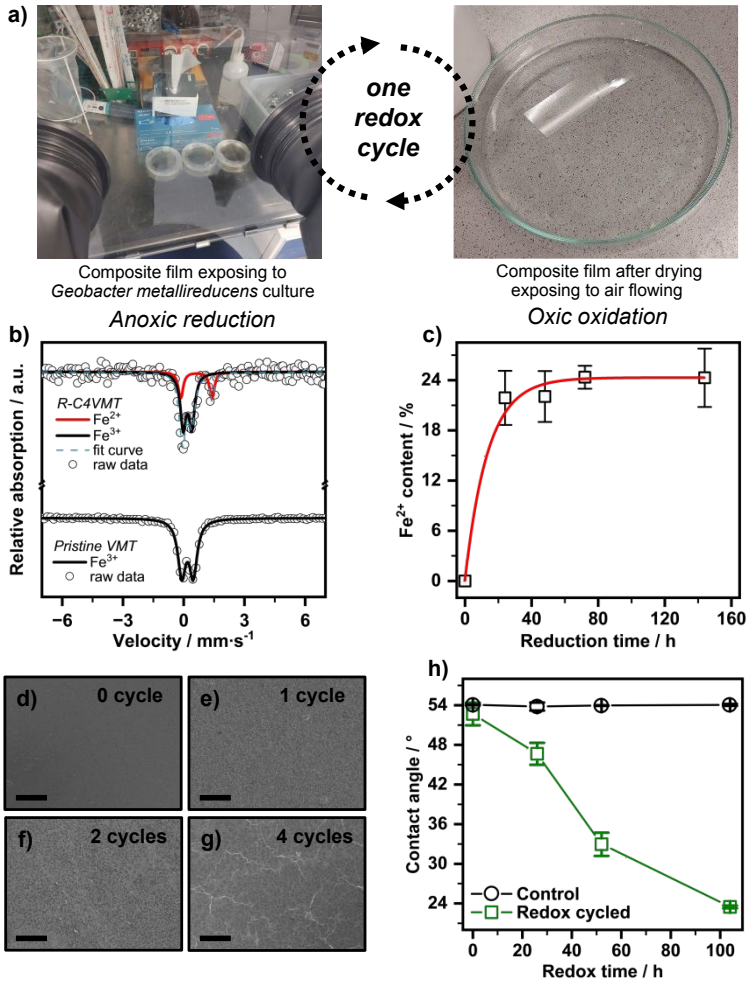

Figure 3. a) Redox cycling of the C4VMT/PNAT$_{30}$ Bragg-stack coating on a PLA substrate: The film is first immersed in a culture medium inoculated with *Geobacter metallireducens* under strictly anaerobic conditions to induce biotic reduction of structural Fe(III) of C4VMT nanosheets. Subsequently the film is removed from the medium and exposed to atmosphere. b) Mößbauer spectra of the C4VMT nanosheets after being suspended in the culture medium with *Geobacter metallireducens*, showing the partial reduction of structural Fe(III) to Fe(II). c) Monitoring of the Fe(II) fraction with time that the coating was suspended in the bacterial medium. d–g) Scanning electron microscope (SEM) images of the surface of the d) pristine barrier coating and after e) 1, f) 2, and g) 4 redox cycles (scale bars: 100 µm). h) Change of contact angle of the coating surface with water with the numbers of exposure to culture media with and without inoculation of *Geobacter metallireducens*.

View Article Online
DOI: 10.1039/D6LP00059B

SEM (Figure 3d–g) images of the coating surface furthermore indicated increasing morphological changes of the polymer with successive redox cycles. Specifically, the pristine surface appeared compact and smooth, without detectable defects or cracks before redox cycling. Already after the first redox cycle, nanoscale roughening and shallow pits developed (Figure 3e and 3f), indicating surface restructuring or morphological changes as redox alteraion proceeds. After four cycles, interconnected cracks became evident throughout the entire surface (Figure 3g). These microstructural changes observed in the coatings are consistent with the built-in chemical formation of a more hydrophilic surface. Oxidation of the thioether bonds into sulfoxides of $PNAT_{30}$ leads to a more hydrophilic surface that is expected to increase swelling with water and this in turn causes appreciable mechanical stress causing the cracking (Fig. 3 d-g). SEM images (Fig. S8) of the surface of samples exposed four times to the culture medium without inculation of Geobacter metallireducens and hence without oxidative hydrophilization, show no visible cracking. This indicates that the mechanical stress induced by the limited swelling of pristine $PNAT_{30}$ causes no crack formation. The increased hydrophilicity with redox cycling of the coating was moreover evidenced by the progressive and substantial decrease in the contact angle of the composite film surface (Figure 3h) that had been oxidized after anoxic microbial reduction followed by air exposure. The pristine nanocomposite coating showed a large contact angle with water of 54° as expected for a hydrophobic $PNAT_{30}$ matrix (Figure S4). The contact angle decreased with each redox cycle becoming as low as 24° after 4 cycles (Figure 3h, Figure S5 – S7) indicating a substantially more polar surface. This change may not be attributed to the exposure to culture media alone (Figure 3h, control) as this does not show a change of contact angle. The inoculation of *Geobacter metallireducens* triggering reduction of structural Fe(III) was essential for observing the change in contact angle. The polar surface of the coating is expected to increase post-use wettability that may facilitate subsequent microbial attachment. The change in contact angle for the coating is,

View Article Online
DOI: 10.1039/D6LP00059B

however, primarily driven by the built-in chemical formation of an abiotic corona rather than external factors such as passive adsorption or polymer relaxation.[55, 56] While barrier performance was only measured for the pristine coating in the present study, the observed increase in hydrophilicity, surface roughening, and crack formation after redox cycling would be expected to impair the compact Bragg-stack architecture and thus deteriorate barrier performance.

CONCLUSION

The primary goal of this study was to modify the hydrophobic coating surface as required for barrier performance during usage into a hydrophilic surface that fosters eco corona formation and ultimately biodegradation of the complete packaging including the PLA substrate. As quantitative oxidation is not relevant, fluxes and timescales are therefore unconnected.

The Bragg-stack nanocomposite coatings developed in this work demonstrate that fully delaminated natural VMT nanosheets can be used to convert intrinsically poor-barrier, biodegradable polyester substrates into high-performance food-packaging films while simultaneously programming their surface for environmentally triggered hydrophilization. The C4VMT/$PNAT_{30}$ coatings form highly ordered one-dimensional Bragg-stacks with nanometre-scale polymer interlayers, yielding oxygen and water vapor transmission rates that match demanding food-packaging benchmarks at elevated relative humidity despite a coating thickness of only about 2 μm. Through redox cycling of structural Fe(III)/Fe(II) in VMT, VMT-mediated ROS oxidize thioether units in $PNAT_{30}$ to sulfoxides is inferred from complementary FTIR, Raman, and solid-state NMR analyses and supported by literature reports on Fe-bearing clay redox chemistry.[24, 25, 29,30] This molecular-level oxidation translates into macroscopic surface restructuring forming cracks and a pronounced decrease in water contact angle from initially hydrophobic values to around 24°, indicating the in situ formation of a more hydrophilic coating

View Article Online
DOI: 10.1039/D6LP00059B

surface that may facilitate subsequent microbial attachment and eco-corona development on MPs derived from such coatings. The key innovation is the integration of barrier enhancement and redox-responsive sulfur chemistry within a single mineral–polymer architecture. This approach offers a materials design concept for packaging that protects food during use but, after release into fluctuating anoxic/oxic environments, becomes more wettable and microbially accessible, thereby helping to reconcile performance requirements with an accelerated and more controllable end-of-life fate. Questions regarding the environmental toxicity, persistence, and possible release of coating components, particularly after weathering or redox-activated structural alteration, were beyond the scope of the present study and will require dedicated investigation in future work. Moreover, direct degradation studies will be required to determine whether the observed surface hydrophilization of the coating translates into accelerated degradation of the coated polymer system under specific environmental conditions. In conclusion, our work provides a promising approach for developing high-performance and environmentally friendly food packaging materials.

MATERIALS AND METHODS

Materials

The VMT was obtained from a German importer, Isola, which originates from a mine in Africa (IV-DB-DEU-Uganda-Namekara-2022-V2.pdf). According to the composition given by the supplier, the structural formula of a half unit cell is $[Mg_{0.37}]^{inter}[Mg_{2.44}Fe_{0.46}]^{oct}[Si_{3.15}Al_{0.85}]^{tet}O_{10}(OH)_2$. The cation exchange capacity as measured photometrically via $[Co(en)]^{3+}$ exchange was found to be 186 meq/100 g. Natural VMT flakes were first ground and sieved to sizes < 100 µm size. All other chemicals used were supplied by Sigma Aldrich (LiCl (≥ 99 %), butylamine (≥ 99.5 %), sodium citrate dihydrate (≥ 99 %), L-ascorbic acid (≥ 99 %), citric acid (≥ 99 %).

View Article Online
DOI: 10.1039/D6LP00059B

Cation exchange and delamination

The ground VMT was suspended in 100 mL of a 2 M (or 400 times the CEC) solution of butylamine (C4) titrated with citric acid to pH 7 and refluxed for 24 hours. The high ionic strength inhibits delamination. After five rounds of washing and centrifugation with a 50/50 vol% water/ethanol combination (again, the ethanol concentration inhibits spontaneous delamination), the VMT was dried in a vacuum oven at 70°C. A rational 00l series with a very small coefficient of variation (CV) of 0.13 % indicates complete C4 exchange.[57] Upon suspending C4-vermiculite (C4VMT) in NMF, it spontaneously delaminates to a nematic suspension. Delamination is completed within 24 hours in an overhead shaker at room temperature (RT) and a birefringent suspension is obtained.

Chemical reduction of structural iron in VMT

The C4VMT samples (0.5 g, equivalent to 0.56 mmol structural Fe) were delaminated by resuspending in 20 mL of deoxygenated, Ar-saturated water (concentration of the suspension 2 wt%). To this suspension, 20 mL of a 100 mM ascorbate solution was added, yielding a total volume of 40 mL with a 50 mM ascorbate concentration, equivalent to 2.0 mmol ascorbate in the suspension. Ascorbate is applied at a molar excess of approximately 3.6 times relative to structural Fe. After 12 h, 30 % of the structural Fe(III) was reduced to Fe(II) as evidenced by Mößbauer spectroscopy (Figure S3).

Reduction of structural iron in VMT by Geobacter metallireducens

Geobacter metallireducens[58] is a metal-reducing bacterium capable of growth via complete oxidation of organic substrates coupled to dissimilatory Fe(III) reduction. The strain used in this study (GS-15 / ATCC 53774 / DSM 7210) was obtained from the Leibniz Institute DSMZ - German Collection of Microorganisms and Cell Cultures in Braunschweig, Germany. *G. metallireducens* was cultivated for biomass generation under strictly anoxic conditions in Bellco 27 mL headspace

View Article Online
DOI: 10.1039/D6LP00059B

vials sealed with 20 mm crimp stoppers using the DSMZ medium 579. The medium was prepared with (per L): 13.70 g ferric citrate monohydrate, 1.50 g NH_4Cl, 0.60 g $NaH_2PO_4 \cdot H_2O$, 0.10 g KCl, and 2.50 g sodium acetate. After autoclaving and cooling under an N_2/CO_2 (80:20, v/v) atmosphere, 2.50 g L^{-1} $NaHCO_3$ buffer was added under N_2/CO_2. Subsequently, the following components were added from sterile, anoxic stock solutions: 10 mL L^{-1} vitamin solution (DSMZ medium 141) and 1 mL L^{-1} modified Wollin's mineral solution (DSMZ medium 120). The pH of the final medium was adjusted to 6.7–7.0. Growth of the culture to an OD_{600} of ~1.6 was done over 10 days at 30 °C in the dark.

Microbial VMT reduction incubations

Next to standard growth media described above, separate stocks of DSMZ medium 579 were prepared without ferric citrate as electron acceptor. Here, structural Fe(III) of the VMT nanofiller incorporated into the C4VMT/$PNAT_{30}$ Bragg-stack coatings served as the sole electron acceptor. The coatings on PLA films (~3 cm^2) were placed into standard petri dishes containing 20 mL of ferric citrate-omitted culture medium and inoculated with 1 ml of pre-grown cells of the active culture of *G. metallireducens*. Incubation was carried out within an anaerobic chamber (Mecaplex, Grenchen, CH) flushed with N_2 to allow for biotic reduction of iron in the nanosheets. For a single reduction cycle, nanosheets comprised within the coating were incubated for 24 h at room temperature in the anoxic chamber. Subsequently, the coated PLA films were removed from the culture medium and exposed to ambient air for 2 h to induce Fenton-type oxidative reactions. Reduction cycles 2 to 4 were performed by repeating the cycling two to four times, respectively, by re-exposing the coated PLA films to fresh biomass of *G. metallireducens* in fresh ferric citrate-omitted culture medium within the anaerobic chamber. After final re-oxidation, nanosheets were dried at 30 °C in the dark before downstream analysis.

View Article Online
DOI: 10.1039/D6LP00059B

Synthesis of poly(N-acryloylthiomorpholine) ($PNAT_{30}$)

$PNAT_{30}$ was prepared following established procedures.[59] Briefly, 2-(butylthiocarbonothioylthio)-propanoic acid (PABTC, 2.12 mL of a 0.5 M solution in 1,4-dioxane, 1.06 mmol), N-acryloylthiomorpholine (5.0 g, 31.8 mmol), and the radical initiator VA-044 (0.86 mL of a 20 $mg \cdot mL^{-1}$ solution in Milli-Q water, 53.2 µmol) and 1,3,5-trioxane (20 mg) were combined in a 5 mL microwave vial and sealed with a rubber septum. After deoxygenation by argon bubbling for 20 min, the vial was placed in a preheated oil bath at 70 °C and stirred for 24 h, until monomer conversion was confirmed by ^1H NMR (0.1 mL aliquot in $CDCl_3$). The reaction mixture was cooled to room temperature and precipitated in diethyl ether (300 mL). The product was dried under reduced pressure at 40 °C for 24 h. A number average molar mass (M_n) of 1.8 kg mol^{-1} and a dispersity (Đ) 1.13 was determined by size exclusion chromatography (SEC) (eluent: DMAc + 0.21 wt.% LiCl, calibration with PEO standards). The corresponding SEC trace and an ^1H-NMR spectrum of the polymer are given in the supplementary information (Figure S9).

Fabrication of Bragg-stack nanocomposite barrier coating

The C4VMT/$PNAT_{30}$ suspension were applied on PLA films as a wet coat, which was prepared by mixing a 10 wt% $PNAT_{30}$ solution in DMF with a 5 wt% VMT dispersion in a mixture of γ-butyrolacton and NMF (γ -BL/NMF: 90:10) followed by mixing overnight on an overhead mixer.[11] The highly ordered 1D crystalline hybrid Bragg-stack requires a careful, iterative optimization of the clay-to-polymer ratio. The optimum was found for a polymer weight fraction of around 30 wt% corresponding to 47 vol% taking the different densities for polymer and clay into account. A wet coat (6.67 wt% solid content) of 100 µm was applied to a PLA substrate (25 µm supplied by Pütz Folien GmbH) by doctor blading (K Control Coater K202*, RK PrintCoat Instruments Ltd., United Kingdom). The substrate temperature was kept at RT, while the blade speed was 3 cm s^{-1}. The

View Article Online
DOI: 10.1039/D6LP00059B

coated foils were dried overnight at RT followed by drying at 40℃ in a vacuum oven for two days. The coating thickness of 2 μm was determined using a high-accuracy Digimatic micrometer (Mitutoyo, Japan) with a measuring range of 0–25 mm and a resolution of 0.0001 mm.

Mößbauer spectroscopy

The evolution of microbial reduction of VMT with time was followed by taking 20 mL of suspension at chosen time steps. The reduced VMT were washed with deionized, de-oxygenated and Ar-saturated water and centrifuged in inert atmosphere in a glovebox. Some 0.20 g of powder were packed in the glovebox into a circular sample holder. Samples were sealed with Kapton film to mitigate re-oxidation and were immediately measured.

^{57}Fe Mößbauer spectra were recorded in transmission geometry at 295 ± 2 K within less than 12 h sampling time. Mößbauer spectra were collected with a configuration designed for high-resolution measurements. The setup consisted of a WissEl Mößbauer Drive System MR-360, an MA-260 velocity transducer for precise and controlled motion of the ^{57}Co(Rh) source (activity: ~50 mCi), and a KETEK silicon drift detector AXAS-M. The gain and shaping time constants were optimized experimentally. Data was collected using a CMCA-550 module in MCS [WINDOW] mode, enabling the selective detection of the 14.4 keV Mößbauer line. Calibration was carried out using a ^{57}Fe-enriched metallic foil. Measurements were taken at RT. The sinusoidal velocity waveform for the source motion was generated by a DFG-1000 digital function generator, which was synchronized with the CMCA-550 channel sweep. (Spectral data were processed and analysed with MossA software to ensure accurate alignment and energy calibration.[60] Lorentzian line shapes were applied to fit the doublets. No constraint was applied.

X-ray diffraction

View Article Online
DOI: 10.1039/D6LP00059B

Cu K_α radiation (λ = 1.54187 Å) was used to collect XRD data applying a Bragg–Brentano-type diffractometer (Empyrean, Malvern Panalytical BV, The Netherlands) fitted with a PIXcel-1D detector. The HighScore Plus program from Malvern Panalytical was used for peak search.

Small angle X-ray scattering

A "Double Ganesha AIR" (SAXSLAB/Xenocs) was used to record small angle X-ray scattering (SAXS) data. This lab-based system uses a rotating copper anode (MicroMax-007 HF, Rigaku Corporation, Japan) to produce a focused X-ray beam and a position-sensitive detector (PILATUS 300K, Dectris). The scattering vector range q = 0.0024 – 1.05 A^{-1} was covered. The C4VMT suspensions were added into 1 mm glass capillaries (Hilgenberg, code 4007610) for measuring. The data were circularly averaged and adjusted to account for the measurement duration, sample thickness, and incident beam. For background subtraction, a capillary filled with solvent was measured. Scatter (version 2.5) was used for further examination.

Static light scattering

A HORIBA LA-950 SLS device was applied to record the hydrodynamic radii distribution of aqueous dispersions by static light scattering (SLS). The solid phase's refractive index was assumed to be 1.5.

Transmission electron microscopy

Cross-sectional transmission electron microscopy (TEM) images were measured by employing a JEOL-JEM-2200FS (JEOL GmbH, Germany) microscope. Cross sections of the nanocomposite coating were prepared by using a JEOL EM-09100IS Cryo Ion Slicer (JEOL GmbH, Germany).

Fourier-transform infrared spectroscopy

View Article Online
DOI: 10.1039/D6LP00059B

For Fourier-transform infrared spectroscopy (FTIR) measurements, a Jasco FTIR 6100 spectrometer was applied.

Raman spectroscopy

Raman spectra were acquired in confocal geometry using a Horiba Jobin Yvon Raman spectrometer equipped with an Olympus BX41 microscope (50x magnification) and a He-Ne-Laser (11.5 mW laser power, $\lambda = 633$ nm). The spectra were recorded in the spectral range of 50 to 3500 cm^{-1} by summation of 20 individual spectra (5 s exposure time) using the Labspec 5 software.

Solid-state NMR spectroscopy

The polymer samples before and after oxidation were measured with a spectrometer Bruker Avance III 400 (Magnetic Field 9.4 T). The solid state ^{13}C NMR MAS spectra were obtained using a ramped cross-polarization (CP) experiment, where the nutation frequency on the proton channel varied linearly by 50 %. The samples were spun at 20.0 kHz in a 3.2 mm MAS triple resonance probe. The corresponding nutation frequency on the ^{13}C channel and the contact time were adjusted to 70 kHz and 1 ms, respectively. During acquisition proton broadband decoupling was applied using a spinal-64 sequence with a nutation frequency = 60 kHz. The ^{13}C spectra are referenced indirectly with respect to tetramethylsilane (TMS) using adamantane as secondary reference.

Oxygen transmission rate

Oxygen transmission rate (OTR) was determined on a Mocon OX-TRAN 2/21 M10x system (Mocon Inc., USA) with a lower detection limit of 5×10^{-4} cm^3 m^{-2} day^{-1} atm^{-1}. The measurements were performed at 23 ℃ and 65 % RH. A mixture of 98 vol% nitrogen and 2 vol% hydrogen was used as the carrier gas and pure oxygen as the permeant (＞99.95 %, Linde Sauerstoff 3.5).

Water vapor transmission rate

View Article Online
DOI: 10.1039/D6LP00059B

Water vapor transmission rate (WVTR) was determined on a HiBarSens HBS 2.0 HT (Sempa Systems GmbH, Dresden, Germany) with a lower detection limit of 10^{-6} g m^{-2} day^{-1}. The tests were conducted at 23 °C at a relative humidity of 75 %.

Size exclusion chromatography (SEC)

Size-exclusion chromatography (SEC) of polymers was performed on an Agilent system (series 1200) equipped with a PSS degasser, a G1310A pump, a G1362A refractive index detector and a PSS GRAM 30 and 1000 column with DMAc (+ 0.21 wt.% LiCl) as eluent and a flow rate of 1 mL min^{-1}. The column oven was set to 40°C and poly(ethylene oxide) (PEO) standards were used for calibration.

AUTHOR INFORMATION

Corresponding Author

***Josef Breu** − Bavarian Polymer Institute and Department of Chemistry, University of Bayreuth, Universitätsstr. 30, 95440 Bayreuth, Germany; orcid.org/0000-0002-2547-3950; E-mail: Josef.breu@uni-bayreuth.de

***Tillmann Lueders** − University of Bayreuth, Ecological Microbiology, Bayreuth Center of Ecology and Environmental Research (BayCEER), 95440 Bayreuth, Germany; orcid.org/0000-0002-9361-5009; E-mail: tillmann.lueders@uni-bayreuth.de

***Johannes C. Brendel** − University of Bayreuth, Macromolecular Chemistry I, 95440 Bayreuth, Germany. orcid.org/0000-0002-1206-1375; E-mail: johannes.brendel@uni-bayreuth.de

Authors

View Article Online
DOI: 10.1039/D6LP00059B

Xiong Xiong − Bavarian Polymer Institute and Department of Chemistry, University of Bayreuth, Universitätsstr. 30, 95440 Bayreuth, Germany

Sulari Anthony − University of Bayreuth, Ecological Microbiology, Bayreuth Center of Ecology and Environmental Research (BayCEER), 95440 Bayreuth, Germany

Juliane Eberhardt − University of Bayreuth, Macromolecular Chemistry I, 95440 Bayreuth, Germany

Sabine Rosenfeldt − University of Bayreuth, Physical Chemistry I, Universitätsstr. 30, 95440 Bayreuth, Germany

Daniel Friedrich − Bavarian Polymer Institute and Department of Chemistry, University of Bayreuth, Universitätsstr. 30, 95440 Bayreuth, Germany

Stefan Peiffer − University of Bayreuth, Bayreuth Center of Ecology and Environmental Research (BayCEER), Department of Hydrology, Bayreuth 95440, Germany

Funding Sources

The project has been funded by the Deutsche Forschungsgemeinschaft (DFG, German Research Foundation) – project number 391977956 – SFB1357/C02, B01 and A06. JCB further thanks the German Science Foundation (DFG) for funding within the Heisenberg-Programme (Project-ID: 517761335).

Notes

The authors declare no competing financial interest.

View Article Online
DOI: 10.1039/D6LP00059B

ACKNOWLEDGMENT

The project has been funded by the Deutsche Forschungsgemeinschaft (DFG, German Research Foundation) – project number 391977956 – SFB1357/C02, B01 and A06. JCB further thanks the German Science Foundation (DFG) for funding within the Heisenberg-Programme (Project-ID: 517761335). The support from the keylabs (Mesoscale Characterization: Scattering Techniques, Surface and Interface Characterization, and Polymer Additives and Fillers) of the Bavarian Polymer Institute (BPI) at University of Bayreuth is much appreciated. Marco Schwarzmann is thanked for preparing the transmission electron microscopy and scanning electron microscopy images, Beate Bojer is thanked for solid-state NMR measurement, and Daniel Hohenberger for Mößbauer spectroscopy measurement. We thank Prof. Dr. A. Lerf for making the Mößbauer source available.

REFERENCES

(1) Geyer, R.; Jambeck, J. R.; Law, K. L. Production, use, and fate of all plastics ever made. *Science Advances* **2017**, *3* (7), e1700782. DOI: 10.1126/sciadv.1700782.

(2) Jambeck, J. R.; Geyer, R.; Wilcox, C.; Siegler, T. R.; Perryman, M.; Andrady, A.; Narayan, R.; Law, K. L. Plastic waste inputs from land into the ocean. *Science* **2015**, *347* (6223), 768. DOI: 10.1126/science.1260352.

(3) Andrady, A. L. Weathering and fragmentation of plastic debris in the ocean environment. *Marine Pollution Bulletin* **2022**, *180*, 113761. DOI: 10.1016/j.marpolbul.2022.113761.

(4) de Souza Machado, A. A.; Kloas, W.; Zarfl, C.; Hempel, S.; Rillig, M. C. Microplastics as an emerging threat to terrestrial ecosystems. *Global Change Biology* **2018**, *24* (4), 1405. DOI: 10.1111/gcb.14020.

(5) Eerkes-Medrano, D.; Thompson, R. C.; Aldridge, D. C. Microplastics in freshwater systems: A review of the emerging threats, identification of knowledge gaps and prioritisation of research needs. *Water Research* **2015**, *75*, 63. DOI: 10.1016/j.watres.2015.02.012.

(6) Scheurer, M.; Bigalke, M. Microplastics in Swiss Floodplain Soils. *Environmental Science & Technology* **2018**, *52* (6), 3591. DOI: 10.1021/acs.est.7b06003.

(7) Ramsperger, A. F. R. M.; Bergamaschi, E.; Panizzolo, M.; Fenoglio, I.; Barbero, F.; Peters, R.; Undas, A.; Purker, S.; Giese, B.; Lalyer, C. R.; et al. Nano- and microplastics: a comprehensive

View Article Online
DOI: 10.1039/D6LP00059B

review on their exposure routes, translocation, and fate in humans. *NanoImpact* **2023**, *29*, 100441. DOI: 10.1016/j.impact.2022.100441.

(8) Beaumont, N. J.; Aanesen, M.; Austen, M. C.; Börger, T.; Clark, J. R.; Cole, M.; Hooper, T.; Lindeque, P. K.; Pascoe, C.; Wyles, K. J. Global ecological, social and economic impacts of marine plastic. *Marine Pollution Bulletin* **2019**, *142*, 189. DOI: 10.1016/j.marpolbul.2019.03.022.

(9) Borrelle, S. B.; Ringma, J.; Law, K. L.; Monnahan, C. C.; Lebreton, L.; McGivern, A.; Murphy, E.; Jambeck, J.; Leonard, G. H.; Hilleary, M. A.; et al. Predicted growth in plastic waste exceeds efforts to mitigate plastic pollution. *Science* **2020**, *369* (6510), 1515. DOI: 10.1126/science.aba3656.

(10) Lau, W. W. Y.; Shiran, Y.; Bailey, R. M.; Cook, E.; Stuchtey, M. R.; Koskella, J.; Velis, C. A.; Godfrey, L.; Boucher, J.; Murphy, M. B.; et al. Evaluating scenarios toward zero plastic pollution. *Science* **2020**, *369* (6510), 1455. DOI: 10.1126/science.aba9475.

(11) Dudko, V.; Timmins, R. L.; Khoruzhenko, O.; Röhrl, M.; Greve, C.; Rosenfeldt, S.; Tammelin, T.; Agarwal, S.; Herzig, E. M.; Breu, J. Spontaneous delamination of affordable natural vermiculite as a high barrier filler for biodegradable food packaging. *Materials Advances* **2022**, *3* (24), 9052. DOI: 10.1039/d2ma00734g.

(12) Röhrl, M.; Timmins, R. L.; Ghosh, D.; Schuchardt, D. D.; Rosenfeldt, S.; Nürmberger, S.; Bölz, U.; Agarwal, S.; Breu, J. Green and scalable processing of water-soluble, biodegradable polymer/clay barrier films. *Journal of Applied Polymer Science* **2023**, *140* (37), e54418. DOI: 10.1002/app.54418.

(13) Röhrl, M.; Timmins, R. L.; Rosenfeldt, S.; Schuchardt, D. D.; Uhlig, F.; Nürmberger, S.; Breu, J. Stretchable Clay Nanocomposite Barrier Film for Flexible Packaging. *ACS Applied Materials & Interfaces* **2023**, *15* (18), 22524. DOI: 10.1021/acsami.3c02504.

(14) Basha, R. K.; Konno, K.; Kani, H.; Kimura, T. Water vapor transmission rate of biomass based film materials. *Engineering in Agriculture, Environment and Food* **2011**, *4* (2), 37-42. DOI: 10.1016/S1881-8366(11)80018-2.

(15) Timmins, R. L.; Kumar, A.; Röhrl, M.; Havlíček, K.; Agarwal, S.; Breu, J. High barrier nanocomposite film with accelerated biodegradation by clay swelling induced fragmentation. *Macromolecular Materials and Engineering* **2022**, *307* (6), 2100727. DOI: 10.1002/mame.202100727.

(16) Guebitz, G. M.; Cavaco-Paulo, A. Enzymes go big: surface hydrolysis and functionalisation of synthetic polymers. *Trends in Biotechnology* **2008**, *26* (1), 32-38. DOI: 10.1016/j.tibtech.2007.10.003.

(17) Zhu, X.; Fryd, M.; Barrero, C.; Merali, S.; Fecchio, C.; Valentine, A. M.; Wayland, B. B. Kinetic-mechanistic studies of P. cepacia lipase catalyzed corona charge selective micelle degradation. *Journal of Molecular Catalysis B: Enzymatic* **2016**, *133*, 187-195. DOI: 10.1016/j.molcatb.2016.08.013.

(18) Chamas, A.; Moon, H.; Zheng, J.; Qiu, Y.; Tabassum, T.; Jang, J. H.; Abu-Omar, M.; Scott, S. L.; Suh, S. Degradation Rates of Plastics in the Environment. *ACS Sustainable Chemistry & Engineering* **2020**, *8* (9), 3494. DOI: 10.1021/acssuschemeng.9b06635.

View Article Online
DOI: 10.1039/D6LP00059B

(19) Cussler, E. L.; Hughes, S. E.; Ward, W. J.; Aris, R. Barrier membranes. *Journal of Membrane Science* **1988**, *38* (2), 161. DOI: 10.1016/S0376-7388(00)80877-7.

(20) Moggridge, G. D.; Lape, N. K.; Yang, C.; Cussler, E. L. Barrier films using flakes and reactive additives. *Progress in Organic Coatings* **2003**, *46* (4), 231. DOI: 10.1016/S0300-9440(02)00180-7.

(21) Chen, L.; Zhao, Y.; Chen, T.; Bai, H.; Zhang, T.; Li, H.; An, Q.; Song, S. Correlation of aspect ratio of montmorillonite nanosheets with the colloidal properties in aqueous solutions. *Results in Physics* **2019**, *15*, 102526. DOI: 10.1016/j.rinp.2019.102526.

(22) Falla, W. R.; Mulski, M.; Cussler, E. L. Estimating diffusion through flake-filled membranes. *Journal of Membrane Science* **1996**, *119* (1), 129-138. DOI: 10.1016/0376-7388(96)00106-8.

(23) Pentráková, L.; Su, K.; Pentrák, M.; Stucki, J. W. A review of microbial redox interactions with structural Fe in clay minerals. *Clay Minerals* **2013**, *48* (3), 543-560. DOI: 10.1180/claymin.2013.048.3.10 .

(24) Stucki, J. W. A review of the effects of iron redox cycles on smectite properties. *Comptes Rendus Geoscience* **2011**, *343* (2), 199-209. DOI: 10.1016/j.crte.2010.10.008.

(25) Yu, C.; Ji, W.; Li, X.; Yuan, S.; Zhang, P.; Pu, S. Critical Role of Mineral Fe(IV) Formation in Low Hydroxyl Radical Yields during Fe(II)-Bearing Clay Mineral Oxygenation. *Environmental Science & Technology* **2024**, *58* (22), 9669-9678. DOI: 10.1021/acs.est.3c09986.

(26) Celina, M. C. Review of polymer oxidation and its relationship with materials performance and lifetime prediction. *Polymer Degradation and Stability* **2013**, *98* (12), 2419-2429. DOI: 10.1016/j.polymdegradstab.2013.06.024.

(27) Sajiki, J.; Yonekubo, J. Leaching of bisphenol A (BPA) to seawater from polycarbonate plastic and its degradation by reactive oxygen species. *Chemosphere* **2003**, *51* (1), 55-62. DOI: 10.1016/S0045-6535(02)00789-0.

(28) Geven, M.; d'Arcy, R.; Turhan, Z. Y.; El-Mohtadi, F.; Alshamsan, A.; Tirelli, N. Sulfur-based oxidation-responsive polymers. Chemistry, (chemically selective) responsiveness and biomedical applications. *European Polymer Journal* **2021**, *149*, 110387. DOI: 10.1016/j.eurpolymj.2021.110387.

(29) Fan, Q.; Wang, L.; Fu, Y.; Li, Q.; Liu, Y.; Wang, Z.; Zhu, H. Iron redox cycling in layered clay minerals and its impact on contaminant dynamics: A review. *Science of The Total Environment* **2023**, *855*, 159003. DOI: 10.1016/j.scitotenv.2022.159003.

(30) Purceno, A. D.; Teixeira, A. P. C.; Souza, A. B.; Ardisson, J. D.; de Mesquita, J. P.; Lago, R. M. Ground vermiculite as catalyst for the Fenton reaction. *Applied Clay Science* **2012**, *69*, 87. DOI: 10.1016/j.clay.2012.08.010.

(31) Geiselhart, C. M.; Xue, W.; Barner-Kowollik, C.; Mutlu, H. Degradable Redox-Responsive Polyolefins. *Macromolecules* **2021**, *54* (4), 1775. DOI: 10.1021/acs.macromol.1c00010.

(32) Kilic Boz, R.; Aydin, D.; Kocak, S.; Golba, B.; Sanyal, R.; Sanyal, A. Redox-Responsive Hydrogels for Tunable and "On-Demand" Release of Biomacromolecules. *Bioconjugate Chemistry* **2022**, *33* (5), 839. DOI: 10.1021/acs.bioconjchem.2c00094.

View Article Online
DOI: 10.1039/D6LP00059B

(33) Lin, C.; Hu, H.; Zhu, H.; Luan, Q.; Li, Z.; Wang, J.; Zhu, J. Disulfide-Driven On-Demand Degradation of the PBAT Copolymer: Stable Comprehensive Performance, Long-Term Storage, and Redox-Induced Degradation. *Macromolecules* **2025**, *58* (8), 4170. DOI: 10.1021/acs.macromol.4c02244.

(34) Ziegenbalg, N.; Eberhardt, J.; Städter, S.; Höppener, S.; Stumpf, S.; Brendel, J. C. Monodisperse oxidative-sensitive polymer nanoparticles from dispersion polymerization of N-acryloyl thiomorpholine. *European Polymer Journal* **2023**, *196*, 112258. DOI: 10.1016/j.eurpolymj.2023.112258.

(35) O'Loughlin, J.; Doherty, D.; Herward, B.; McGleenan, C.; Mahmud, M.; Bhagabati, P.; Boland, A. N.; Freeland, B.; Rochfort, K. D.; Kelleher, S. M.; et al. The Potential of Bio-Based Polylactic Acid (PLA) as an Alternative in Reusable Food Containers: A Review. *Sustainability* **2023**, *15* (21), 15312. DOI: 10.3390/su152115312.

(36) Swetha, T. A.; Bora, A.; Mohanrasu, K.; Balaji, P.; Raja, R.; Ponnuchamy, K.; Muthusamy, G.; Arun, A. A comprehensive review on polylactic acid (PLA) – Synthesis, processing and application in food packaging. *International Journal of Biological Macromolecules* **2023**, *234*, 123715. DOI: 10.1016/j.ijbiomac.2023.123715.

(37) Auras, R. A.; Harte, B.; Selke, S.; Hernandez, R. Mechanical, physical, and barrier properties of poly (lactide) films. *Journal of plastic film & sheeting* **2003**, *19* (2), 123-135. DOI: 10.1021/acs.est.1c01512.

(38) Coltelli, M.-B.; Cartoni, F.; Panariello, L.; Aliotta, L.; Gigante, V.; Lazzeri, A. Assessing PLA/PBSA Films for Sustainable Packaging for Moist and Perishable Foods. *Polymers* **2025**, *17* (23), 3093. DOI: 10.3390/polym17233093.

(39) Yue, S.; Zhang, T.; Wang, S.; Han, D.; Huang, S.; Xiao, M.; Meng, Y. Recent Progress of Biodegradable Polymer Package Materials: Nanotechnology Improving Both Oxygen and Water Vapor Barrier Performance. *Nanomaterials* **2024**, *14* (4), 338. DOI: 10.3390/nano14040338.

(40) Yao, S.; Li, X.; Wang, T.; Jiang, X.; Song, Y.; Arp, H. P. H. Soil metabolome impacts the formation of the eco-corona and adsorption processes on microplastic surfaces. *Environmental Science & Technology* **2023**, *57* (21), 8139. DOI: 10.1021/acs.est.3c01877.

(41) Gorski, C. A.; Aeschbacher, M.; Soltermann, D.; Voegelin, A.; Baeyens, B.; Marques Fernandes, M.; Hofstetter, T. B.; Sander, M. Redox Properties of Structural Fe in Clay Minerals. 1. Electrochemical Quantification of Electron-Donating and -Accepting Capacities of Smectites. *Environmental Science & Technology* **2012**, *46* (17), 9360-9368. DOI: 10.1021/es3020138.

(42) Gorski, C. A.; Klüpfel, L.; Voegelin, A.; Sander, M.; Hofstetter, T. B. Redox Properties of Structural Fe in Clay Minerals. 2. Electrochemical and Spectroscopic Characterization of Electron Transfer Irreversibility in Ferruginous Smectite, SWa-1. *Environmental Science & Technology* **2012**, *46* (17), 9369-9377. DOI: 10.1021/es302014u.

(43) Gorski, C. A.; Klüpfel, L. E.; Voegelin, A.; Sander, M.; Hofstetter, T. B. Redox Properties of Structural Fe in Clay Minerals: 3. Relationships between Smectite Redox and Structural Properties. *Environmental Science & Technology* **2013**, *47* (23), 13477-13485. DOI: 10.1021/es403824x.

View Article Online
DOI: 10.1039/D6LP00059B

(44) Neumann, A.; Petit, S.; Hofstetter, T. B. Evaluation of redox-active iron sites in smectites using middle and near infrared spectroscopy. *Geochimica et Cosmochimica Acta* **2011**, *75* (9), 2336-2355. DOI: 10.1016/j.gca.2011.02.009.

(45) Pothanamkandathil, V.; Neumann, A.; Thompson, A.; Gorski, C. A. Redox Properties of Structural Fe in Clay Minerals: 4. Reinterpreting Redox Curves by Accounting for Electron Transfer and Structural Rearrangement Kinetics. *Environmental Science & Technology* **2024**, *58* (44), 19702-19713. DOI: 10.1021/acs.est.4c07835.

(46) Infante Teixeira, L.; Landfester, K.; Thérien-Aubin, H. Selective Oxidation of Polysulfide Latexes to Produce Polysulfoxide and Polysulfone in a Waterborne Environment. *Macromolecules* **2021**, *54* (8), 3659. DOI: 10.1021/acs.macromol.1c00382.

(47) Socrates, G. *Infrared and Raman characteristic group frequencies: tables and charts*; John Wiley & Sons, 2004.

(48) Sjöberg, B.; Foley, S.; Cardey, B.; Fromm, M.; Enescu, M. Methionine oxidation by hydrogen peroxide in peptides and proteins: A theoretical and Raman spectroscopy study. *Journal of Photochemistry and Photobiology B: Biology* **2018**, *188*, 95. DOI: 10.1016/j.jphotobiol.2018.09.009.

(49) Torreggiani, A.; Barata-Vallejo, S.; Chatgilialoglu, C. Combined Raman and IR spectroscopic study on the radical-based modifications of methionine. *Analytical and Bioanalytical Chemistry* **2011**, *401* (4), 1231. DOI: 10.1007/s00216-011-5203-0.

(50) Sobotta, F. H.; Kuchenbrod, M. T.; Gruschwitz, F. V.; Festag, G.; Bellstedt, P.; Hoeppener, S.; Brendel, J. C. Tuneable Time Delay in the Burst Release from Oxidation-Sensitive Polymersomes Made by PISA. *Angewandte Chemie International Edition* **2021**, *60* (46), 24716-24723. DOI: 10.1002/anie.202108928.

(51) Tiquia-Arashiro, S. M.; Pant, D. *Microbial electrochemical technologies*; CRC Press, Taylor & Francis Group, 2020.

(52) Dyar, M. D.; Agresti, D. G.; Schaefer, M. W.; Grant, C. A.; Sklute, E. C. Mössbauer spectroscopy of earth and planetary materials. *Annu. Rev. Earth Planet. Sci.* **2006**, *34* (1), 83-125. DOI: 10.1146/annurev.earth.34.031405.125049.

(53) Manceau, A.; Drits, V. A.; Lanson, B.; Chateigner, D.; Wu, J.; Huo, D.; Gates, W. P.; Stucki, J. W. Oxidation-reduction mechanism of iron in dioctahedral smectites: II. Crystal chemistry of reduced Garfield nontronite. *American Mineralogist* **2000**, *85* (1), 153-172. DOI: 10.2138/am-2000-0115.

(54) Murad, E. Mossbauer spectroscopy of clays, soils and their mineral constituents. *Clay Minerals* **2010**, *45* (4), 413-430. DOI: 10.1180/claymin.2010.045.4.413.

(55) Efimenko, K.; Crowe, J. A.; Manias, E.; Schwark, D. W.; Fischer, D. A.; Genzer, J. Rapid formation of soft hydrophilic silicone elastomer surfaces. *Polymer* **2005**, *46* (22), 9329. DOI: 10.1016/j.polymer.2005.07.046.

(56) Rios, F.; Smirnov, S. Biochemically Responsive Smart Surface. *ACS Applied Materials & Interfaces* **2009**, *1* (4), 768. DOI: 10.1021/am800166t.

View Article Online
DOI: 10.1039/D6LP00059B

(57) Felix Uhlig, A. M. S., Kevin Hagmann, Sabine Rosenfeldt, Josef Breu. Delamination of Vermiculite into Ultrahigh-Aspect-Ratio Nanosheets. *Zeitschrift für anorganische und allgemeine Chemie*. DOI: 10.1002/zaac.70139.

(58) Lovley, D. R.; Giovannoni, S. J.; White, D. C.; Champine, J. E.; Phillips, E. J. P.; Gorby, Y. A.; Goodwin, S. Geobacter metallireducens gen. nov. sp. nov., a microorganism capable of coupling the complete oxidation of organic compounds to the reduction of iron and other metals. *Archives of Microbiology* **1993**, *159* (4), 336-344. DOI: 10.1007/BF00290916.

(59) Sobotta, F. H.; Kuchenbrod, M. T.; Grune, C.; Fischer, D.; Hoeppener, S.; Brendel, J. C. Elucidating preparation-structure relationships for the morphology evolution during the RAFT dispersion polymerization of N-acryloyl thiomorpholine. *Polymer Chemistry* **2021**, *12* (11), 1668-1680. DOI: 10.1039/D0PY01697G.

(60) Prescher, C.; McCammon, C.; Dubrovinsky, L. MossA: a program for analyzing energy-domain Mossbauer spectra from conventional and synchrotron sources. *Journal of Applied Crystallography* **2012**, *45* (2), 329-331. DOI: 10.1107/S0021889812004979.

View Article Online
DOI: 10.1039/D6LP00059B

Sustainable Barrier Coatings for Food Packaging with a Built-in, Redox-activated Trigger for Surface Hydrophilization

Xiong Xiong,[a] Sulari Anthony,[b] Juliane Eberhardt,[c] Sabine Rosenfeldt,[d] Daniel Friedrich, [a] Stefan Peiffer,[e] Johannes C. Brendel,[c] Tillmann Lueders,*[b] Josef Breu*[a]*

a. University of Bayreuth, Bavarian Polymer Institute and Department of Chemistry, Universitätsstr. 30, 95440 Bayreuth, Germany. E-mail: Josef.breu@uni-bayreuth.de

b. University of Bayreuth, Ecological Microbiology, Bayreuth Center of Ecology and Environmental Research (BayCEER), 95440 Bayreuth, Germany. E-mail: tillmann.lueders@uni-bayreuth.de

c. University of Bayreuth, Macromolecular Chemistry I, 95440 Bayreuth, Germany. E-mail: johannes.brendel@uni-bayreuth.de

d. University of Bayreuth, Physical Chemistry I, Universitätsstr. 30, 95440 Bayreuth, Germany

e. University of Bayreuth, Bayreuth Center of Ecology and Environmental Research (BayCEER), Department of Hydrology, Bayreuth 95440, Germany

Data availability statement:

The data supporting this article is presented in the main manuscript or have been included as part of the Supplementary Information.